Persistent Structures in the Turbulent Boundary Layer

Dan Palumbo*
NASA Langley Research Center, Hampton, VA,23681

Chris Chabalko†
Virginia Polytechnic Institute and State University, Blacksburg, VA,24061

Persistent structures in the turbulent boundary layer are located and analyzed. The data are taken from flight experiments on large commercial aircraft. An interval correlation technique is introduced which is able to locate the structures. The Morlet continuous wavelet is shown to not only locates persistent structures but has the added benefit that the pressure data are decomposed in time and frequency. To better understand how power is apportioned among these structures, a discrete Coiflet wavelet is used to decompose the pressure data into orthogonal frequency bands. Results indicate that some structures persist a great deal longer in the TBL than would be expected. These structure contain significant power and may be a primary source of vibration energy in the airframe.

I. Introduction

A better understanding of the nature of the turbulent boundary layer (TBL) and how it interacts with the sidewall of an aircraft may lead to insight into how to prevent the hydrodynamic power in the TBL from coupling into the sidewall and causing subsequent acoustic radiation. To date, most characterizations of the TBL have been in the wavenumber-frequency domain[1,2]. While this is sufficient for many applications, the ensemble averaging that is typically done to produce the spectra obscures the nature of the non-periodic structures that are known to make up the boundary layer. In this paper, two analysis techniques are used to probe time domain TBL data. One is a time interval correlation technique. This analysis is used to locate short intervals of time where high correlation exists between two pressure sensors in the sidewall. The second analysis is the wavelet transform. Wavelet transforms have the potential to decompose the time data based on size and shape, as well as frequency[3]. When the wavelet transform is combined with correlation analysis, a better understanding of the physical characteristics of the persistent structures in the TBL can be formed. Two types of wavelets are used, the continuous Morlet wavelet and the discrete Coiflet[4]. The Morlet wavelet was chosen because of the similarity of the wavelet to structures found with interval correlation. The drawback of the Morlet wavelet is that it does not produce an orthogonal decomposition so that discerning power distributions in the transform becomes difficult, especially in the higher frequencies. The discrete Coiflet transform decomposes the TBL time series into orthogonal components, making analysis of power distribution more straightforward. Once located, the areas of high correlation can be characterized by their persistence, i.e., how long they last.

Data are taken from two series of flight tests. Pressure data were taken from one series of flight tests on an MD 90 aircraft where microphones were flush mounted in adjacent window blanks. Vibration data were taken from a second series of flight tests on a Boeing 757 aircraft where accelerometers were mounted on a long panel located above the windows on the aircraft. The flight tests are described in detail in the following section, followed by descriptions of the time interval correlation analysis, continuous wavelet analysis and discrete wavelet analysis.

---

*Senior Aerospace Engineer, MS 463, Member AIAA

†Research Associate, 320 Femoyer Hall, non-Member

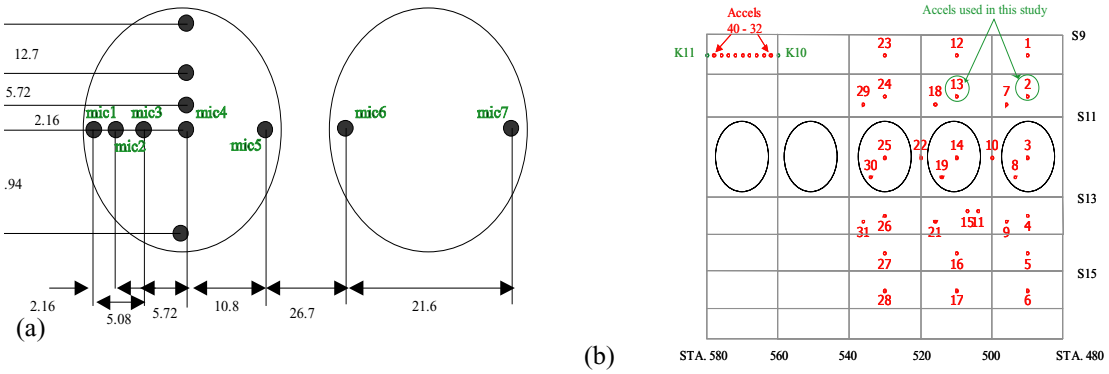

Figure 1. Layout of microphones in window blanks on MD 90 flight test, (a), flow is left to right. Location of accelerometers on 757 flight test, (b), flow is right to left.

II. Flight Tests

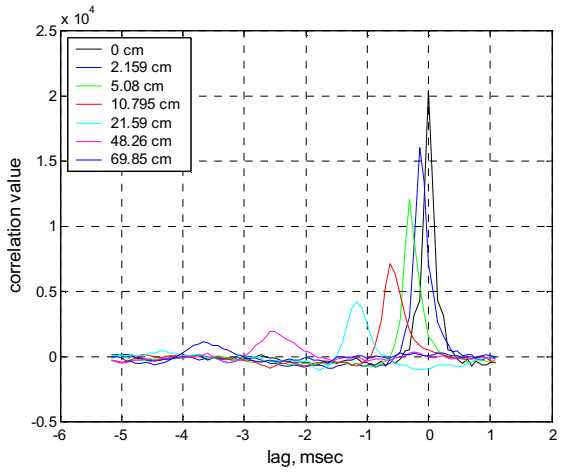

Figure 2. Correlation of microphones 2-7 with microphone 1.

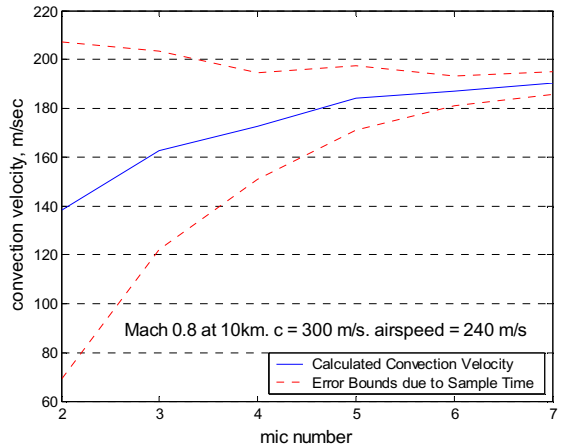

Figure 3. Estimate of convection velocity approaches 190 m/s.

The MD 90 flight tests was conducted by The Boeing Company under contract to NASA as part of the Advanced Subsonic Transport (AST) program. The primary goal of the tests was to evaluate the interior noise field and its dependence on the TBL source. Of primary interest here is the TBL data acquired by the horizontal array of microphones (1 to 7) flush mounted in window blanks as shown in Fig. 1(a). These microphones were 1/4" B&K type 4136. The spacing is as indicated in cm. in Fig. 1(a). The data were acquired at 12.8 kHz for about 30 sec. For the data that will be discussed in the following sections the aircraft was flown at 35,000 ft at 0.8M.

The 757 flight tests were flown on NASA's Aries aircraft[5]. The tests were conducted to evaluate the use of microphone arrays, acoustic holography and source conditioning to measure aircraft cabin noise. Several accelerometers were placed on the aircraft structure to characterize the interior noise vibration sources. Data from two of the accelerometers were used in this study, Fig. 1(b). The accelerometers were Endevco 2250. Data were acquired at 12 kHz. The aircraft was flown at 35,000 ft at 0.8M.

The panels above the windows are unique in that, unlike panels below the window, these panels are not riveted to every ring frame and are over 7 m in length. The increased length of the panel attenuates longitudinal modes, providing a unperturbed look at the TBL forced panel response.

III. Interval Correlation

The interval correlation, R_{int}, can be defined as in Eq. 1 where w is the interval width, d is convection delay and N is the number of samples in the dataset.

$$R_{int}(j) = \sum_{i=j}^{j+w} x(i) \times y(i+d) \qquad (1 \le j \le N-w) \qquad (1)$$

The convection delay is obtained from the standard cross correlation of the microphones as shown in Fig. 2. The correlation falls off rapidly with microphone spacing as expected.

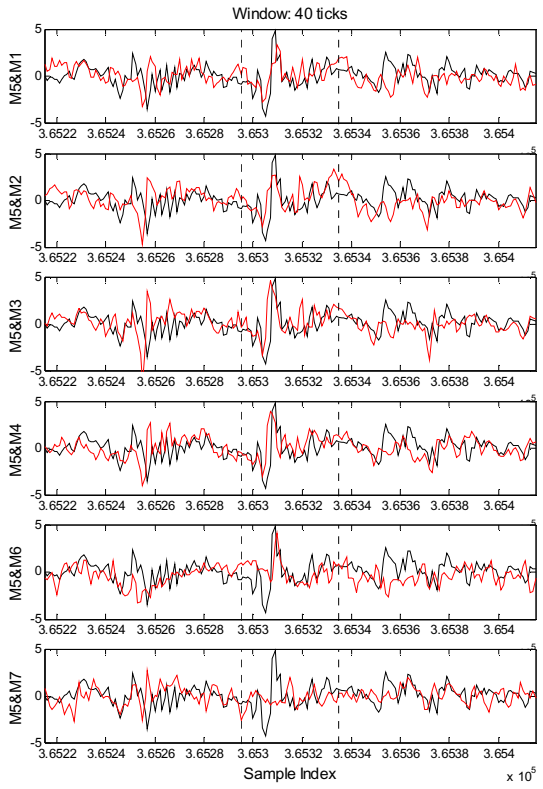

Figure 4. Evolution of persistent structure captured in a 40 sample window referenced to microphone 5.

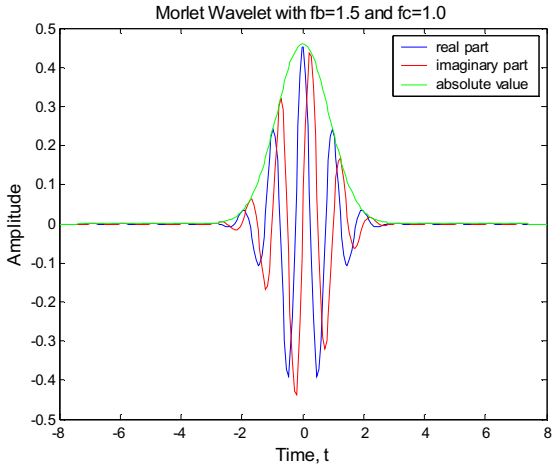

Figure 5. Real and imaginary parts of complex Morlet wavelet for fb=1.5 and fc=1.0.

Taking the peak correlation values and using the associated sensor spacing, an estimate of the convection velocity at the sidewall can be made. As shown in Fig. 3, the convection velocity approaches 190 m/s which is close to the expected value of 80% of airspeed.

The interval width is found by trial and error. A value of 40 samples, 3.1 msec, has worked well for these flight conditions. While an exhaustive search can be done, it has been instructive to select random intervals from a downstream reference sensor and compute the interval correlation with an upstream target sensor. When sections of high correlation are found, those time data are displayed and examined. To help identify random correlations, it is helpful to have several sensors between the reference and target sensors so that the evolution of the structure can be observed.

In Fig. 4 the evolution of a persistent structure is traced from microphone 1 to microphone 7, a total distance of nearly 70 cm. The target sensor was microphone 1 and the reference sensor was microphone 5. The black trace is the reference sensor (mic 5) and the red trace the local sensor (mic n). A prominent structure is clearly seen in the window and is seen to last until microphone 6, almost 50 cm. This structure is about 10 samples long. The size of the structure can be estimated to be about 16 cm., assuming a constant convection velocity for all size structures.

When a persistent structure is located using interval correlation, it is not uncommon to see accompanying correlation outside the interval, especially at longer time scales and lower amplitudes. The example shown in Fig. 4 was chosen as it clearly illustrates this case with two large lobes flanking the structure (3.66526 to 3.653, and 3.6532 to 3.6535) which maintain their shape through microphone 6 up to microphone 7 where correlation outside the interval can still be seen.

To better understand these phenomena, the data were analyzed using the Morlet wavelet in conjunction with the continuous wavelet transform.

IV. The Morlet Wavelet

The Morlet wavelet is described mathematical in Eq. 2 and graphically in Fig. 5.

$$\Psi_{Mor}(t) = \frac{1}{\sqrt{f_b \pi}} e^{i2\pi f_c t} e^{-t^2/f_b} \qquad (2)$$

The Morlet wavelet is characterized by 2 parameters, the wavelet center frequency, f_c, and the envelope shape, f_b. An example wavelet with f_b=1.5 and f_c=1.0 is shown in Fig. 5.

A wavelet is applied to a signal by convolution, e.g.,

$$W(t') = \int s(t)\Psi(t-t')dt\,, \qquad (3)$$

where $s(t)$ is the signal and Ψ the wavelet function. This will return a filtered signal for the particular wavelet applied. To form a continuous wavelet transform (cwt), the wavelet is scaled so that its center frequency is varied over the frequency range of interest.

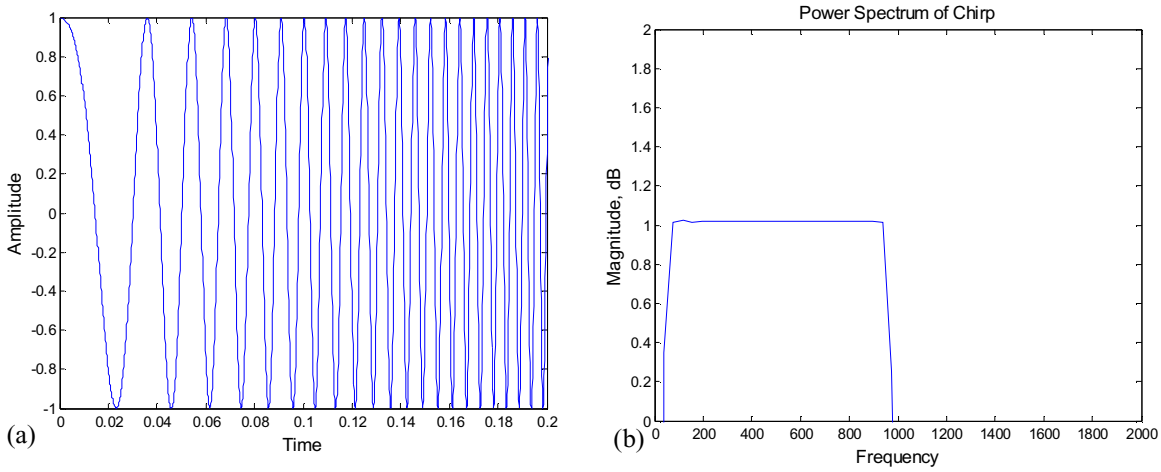

Figure 6. Time history of chirp, (a), and associated power spectrum, (b)

$$C(a,t') = \int s(t)\frac{1}{\sqrt{a}}\Psi(\frac{t-t'}{a})dt \tag{4}$$

The continuous wavelet transform, $C(a,t')$, has frequency, F_a, which corresponds to the scale factor, a, by

$$F_a = \frac{f_c}{a\Delta} \tag{5}$$

where Δ is the signal sample period[4]. The resulting transform has the properties of a time-frequency spectrum as can be illustrated by considering the example of a chirp signal as shown in Fig. 6(a). This chirp varies from 10 Hz to 1 kHz as is clearly seen in its power spectrum in Fig. 6(b).

The continuous wavelet transform of the chirp is shown in Fig. 7(a) with the color axis in dB. One feature that is immediately obvious is the widening bin width with frequency. This characteristic results from the extreme localization of the wavelet as its features are scaled. The high frequency wavelet begins to appear as a delta function, unable to reject frequencies in the neighborhood of its center frequency. Although the Morlet wavelet lacks orthogonality, the shape of the power spectrum is well maintained as shown in Fig. 7(b) where the summed transform is plotted. If the scaling bias is removed from the transform so that the time-frequency plot appears to have a constant bin width and amplitude over the frequency range of the chirp, the total power will become biased towards the higher frequencies. The unscaled transform will be used in the following analyses.

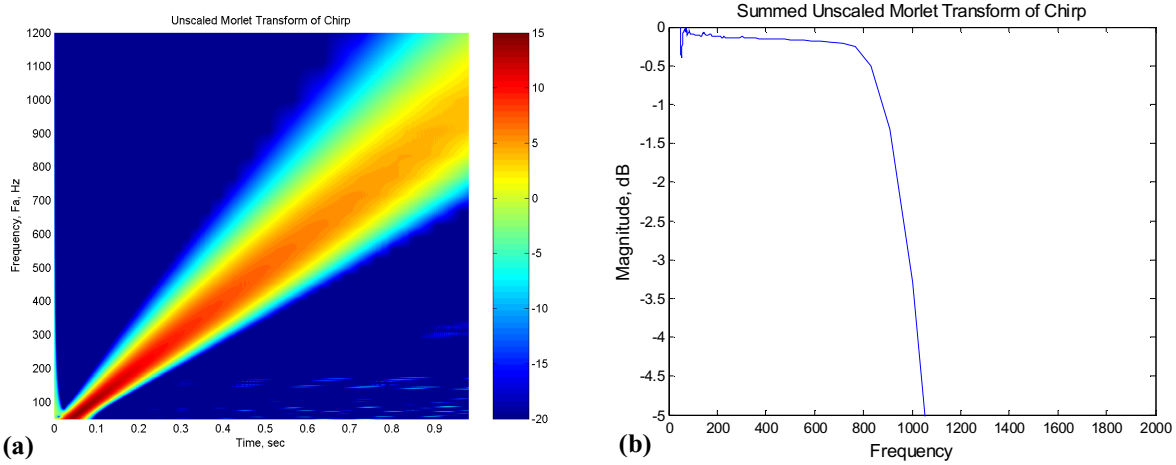

Figure 7. Continuous wavelet transform of chirp using Morlet wavelet, (a). Power spectrum of chirp, (b).

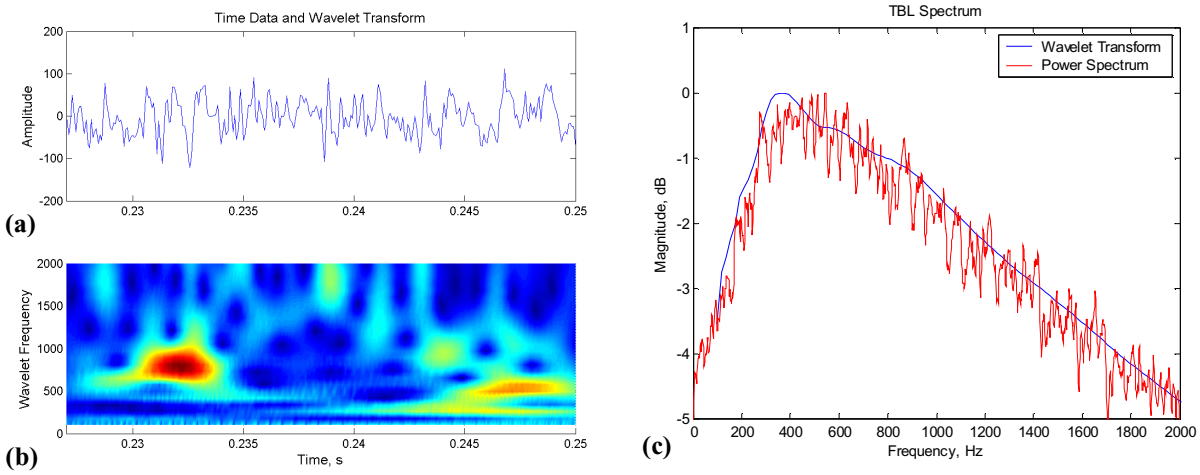

Figure 8. Time history (a) and associated continuous wavelet transform (b) of TBL data. Power spectrum of TBL data compared to summed wavelet transform, (c).

V. The Continuous Wavelet Transform of TBL Data

Applying a continuous Morlet transform to an interval of time data as shown in Fig. 8(a), produces the time-frequency spectrum shown in Fig. 8(b). The wavelet transform is able to locate structures that may be of interest and provide estimates of their approximate frequency content and power. Note that as found with the chirp data, the shape of the power spectrum is maintained, Fig. 8(c), although the absolute magnitude is not.

A. The Occurrence Spectrum

The frequency of occurrence of the structures detected in the wavelet transform can be estimated by Fourier transform of the time component of the wavelet transform.

$$O(a, f_o) = \int C(a, t') e^{-i2\pi f_o t'} dt' \tag{6}$$

In Eq. 6 the delayed time axis of the continuous wavelet transform, $C(a,t')$ is converted to the frequency domain forming the occurrence spectrum, $O(a,f_o)$, the results of which are shown in Fig. 9(a) where the color axis is in dB.

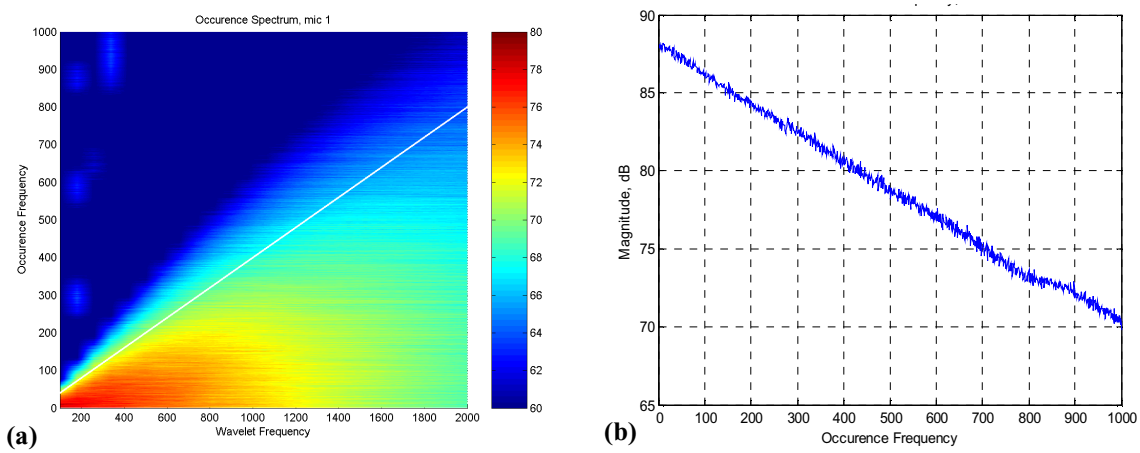

Figure 9. Occurrence spectrum of TBL wavelet transform from microphone 1, (a). Summed occurrence spectrum showing dominance of lower frequencies, (b).

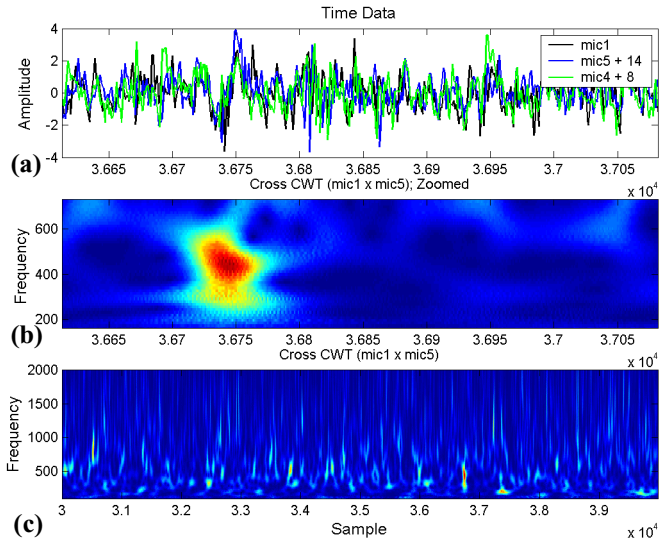

Figure 10. Zoomed time data for microphones 1, 4 and 5, (a), and cross wavelet transform of microphones 1 and 5, zoomed (b), and unzoomed, (c).

The occurrence spectrum apparently retains the low frequency bias of the wavelet transform, however, summing the spectra in the wavelet frequency dimension reveals that the frequency of occurrence is inversely related to the amount of power in the structure, Fig. 9(b). The structures with the most power occur less frequently.

It can also be seen from Fig. 9(a) that the frequency of occurrence is limited by the structure's frequency content, i.e., structures with a frequency of F_a have a frequency of occurrence, f_o, that is below a fraction of F_a. The limiting fraction of occurrence can be seen to be in the neighborhood of 0.4, as plotted in Fig. 9(a).

B. The Cross Wavelet Transform

To locate persistent structures in the TBL, a cross wavelet transform, xwt, can be computed by taking the product of the wavelet transforms of a reference signal to a delayed target signal.

$$X_{1,2}(a,t') = C_1(a,t') \times C^*_2(a,t'-d) \qquad (7)$$

As in Eq. 1, d, in Eq. 7 is the delay as determined by sensor spacing and convection velocity.

The xwt between microphones 1 and 5 is shown in Fig. 10(c). An area of high correlation around 3.675×10^4 samples is expanded in Fig. 10(b). The corresponding time histories are shown in Fig. 10(a). The time history of microphone 4 is plotted in Fig. 10(a) as well to verify the existence of a persistent structure as detected by the cross wavelet transform. The xwt is thus shown to detect persistent structure in the TBL and classify the structures as to their frequency content and size.

The occurrence spectrum can be formed from the xwt as shown in Fig. 11(a). The occurrence spectrum of the xwt is similar in nature to the occurrence spectrum of the cwt with the expected result that the magnitudes are decreased due to the decay and phase shift of the structure. In addition, not all structures are detected at a point in their lifetime such that a persistent characteristic can be found between the reference and target sensors, if it existed at all. The relationship between power and occurrence frequency in the xwt is similar to that in the cwt with the exception that the levels are about 10 dB down, Fig. 11(b). Given that a structure must exist before it can persist, the persistent structures detected by the xwt have the same relative relationship of occurrence frequency limit to wavelet frequency as do the structures detected by the cwt, i.e., the upper limit to occurrence frequency is about $0.4F_a$.

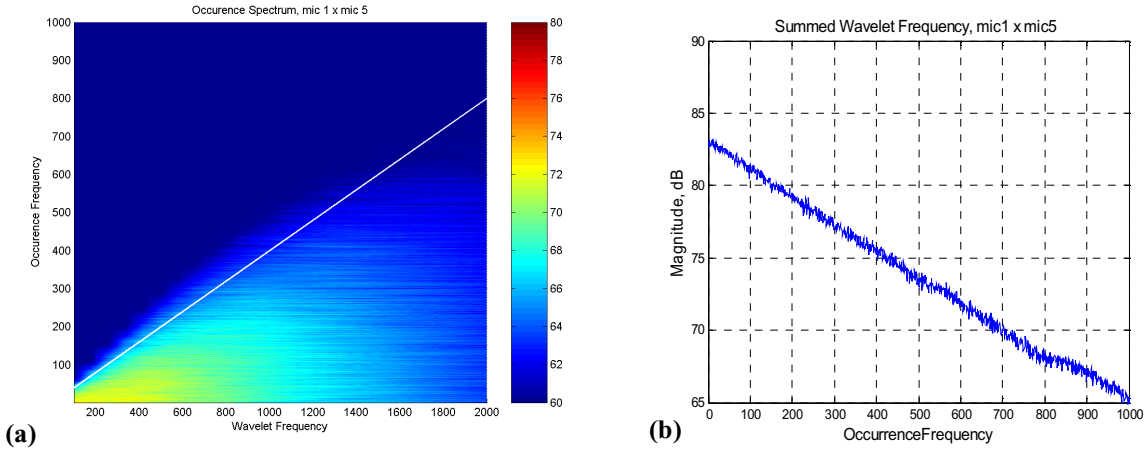

Figure 11. Occurrence spectrum of cross wavelet transform for microphones 1 and 5 (a). Summed cross occurrence spectrum retains dominance of low frequencies

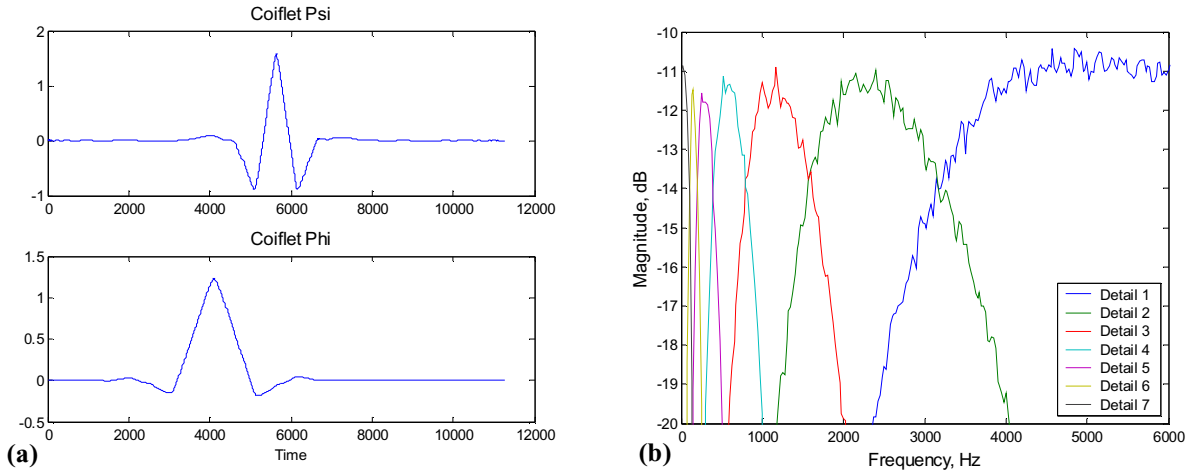

Figure 12. Coiflet detail waveform, psi, and approximation waveform, phi, (a). Frequency bands for N=6 wavelet decomposition of random noise using coiflets.

VI. The Coiflet

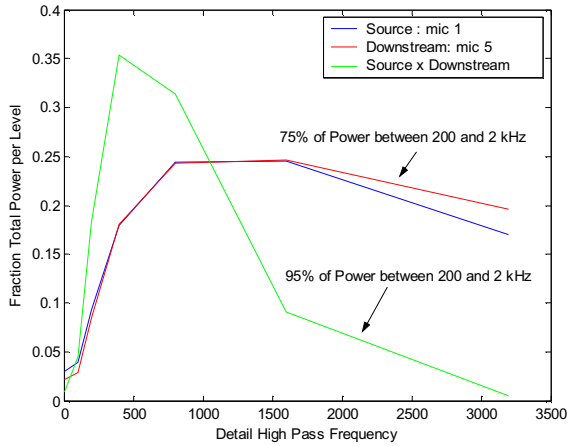

Figure 13. Redistribution of coherent power in coiflet transform, source signals, - and -, and propagated product, -.

The coiflet is composed of a pair of wavelets termed the Psi, or detail, wavelet, and the Phi, or approximation, wavelet, Fig. 12(a). The coiflet pairs work much like high pass and low pass filters with the Psi component returning the higher frequencies and the Phi component the lower frequencies. The detail and approximation results are orthogonal to each other. A discrete wavelet transform, dwt, is constructed by recursively decomposing the signal into details and approximations starting at the higher frequencies and ending with the final approximation covering the lowest band. The power bands of a coiflet dwt of a random signal are shown in Fig. 12(b). The coiflet is thus useful for examining signal content in particular frequency bands.

One drawback of this analysis technique is the overlap of the adjacent bands. In order to capture persistent structures in the filtered time domain, the power bands must completely contain the frequency content of the structure. Even if a power band bridges a frequency band in which persistent structures are expected to occur, the amount of overlap between adjacent bands and the bands' orthogonality to each other acts to tear the structures apart. For example, detail 4 in Fig. 12(b) bridges the frequency band of 200 Hz to 600 Hz that can contain a lot of structure, see Fig. 10(c). However, the overlap of details 3 and 5 act to decompose the structures into unrecognizable signals, making propagation analysis impossible.

The coiflet dwt can be used to estimate the power in persistent structures. The power fraction in a N=6 coiflet dwt of microphones 1 and 5 is compared to the power fraction in the product of microphone 1 delayed and microphone 5 in Fig. 13. A shift in power from the upper to lower frequencies is clearly seen. The frequency range of 200 to 2 kHz is the range in which persistent structures are most often observed.

VII. TBL Forced Panel Vibration

One of the difficulties in sensing TBL data with microphones is the introduction of noise into the data caused by the microphones' interaction with the flow. The vibration data returned from the accelerometers 2 and 13 (Fig. 1(b)) mounted on the long panel above the window line during the 757 flight test is unique in that it provides a view of pure TBL forced panel vibration that is unobscured by panel modes. While these data cannot provide a better estimation of the source pressure field in total, they can provide a very good estimate of that part of the source pressure that is able to transfer energy into the panel.

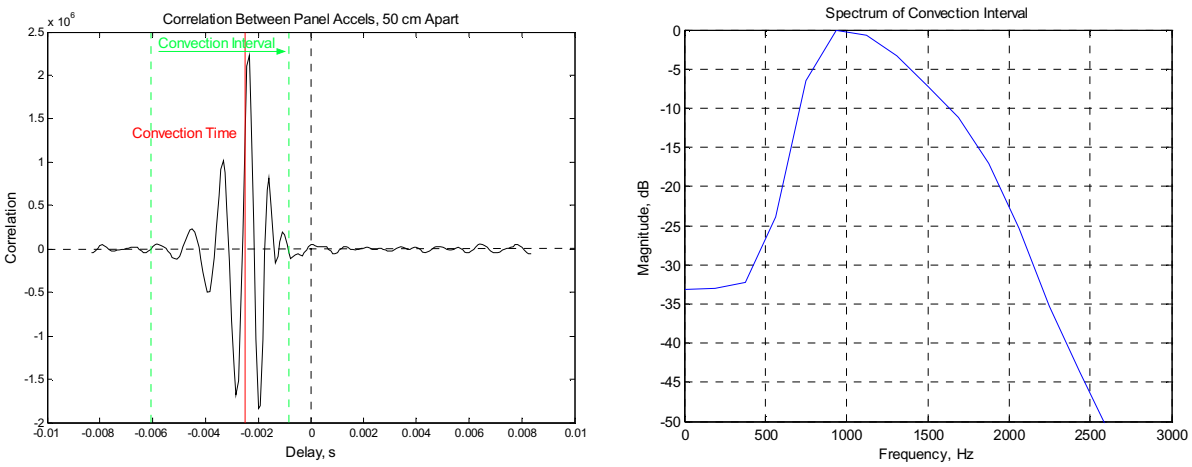

Figure 14. Correlation between accelerometers showing convection interval, (a), and spectrum of convection interval, (b).

The cross correlation between accelerometers 2 and 13 is shown in Fig. 14(a). The convection time between the accelerometers is marked. This delay was estimated using the accelerometer separation, 50 cm., and an approximation for the convection velocity of 0.8 of the airspeed, 0.8M. Lower frequencies are seen to lag the higher frequencies in a convection interval which encompasses the area of high correlation. Note that this interval, at 5 msec, is almost twice the interval size used in Fig. 4 and several times that of observed structures. The frequency content of the convection interval is shown in Fig. 14(b) to go from 600 Hz to 1900 Hz at the -20 dB level.

The cwt of the upstream accelerometer (accel 2) is shown in Fig. 15(a) for a time period of 0.2 seconds. The cwt of the panel vibration data is very similar to that of the flush mounted microphones, Fig. 8(b), above 500 Hz. The accelerometer data is remarkable in the absence of energy below 500 Hz. Either the boundary layer does not have energy in this frequency range for this particular location and flight condition, or, the energy is present, but not able to couple into the panel. In the former case, the microphone data becomes suspect because of the similarity of flight conditions and sensor locations. The likelihood of the latter case is not known as of this writing. The occurrence spectrum for accelerometers 2 and 13 is shown in Fig. 15(b). The concentration of energy between 600 and 1800 Hz is apparent. As found with the microphone data, the low rate structures carry more energy than the higher rate structures. Without the lower frequency wavelet energy, the occurrence frequency limit appears to be close to 0.6 F_a rather than the 0.4 F_a derived with the microphone data. It is most likely this limit is frequency dependent.

With the exception of the absence of low frequency response in the accelerometer data, these results compare favorably with the results obtained with the flush mounted microphones, lending credibility to the conclusions that are drawn based on the data.

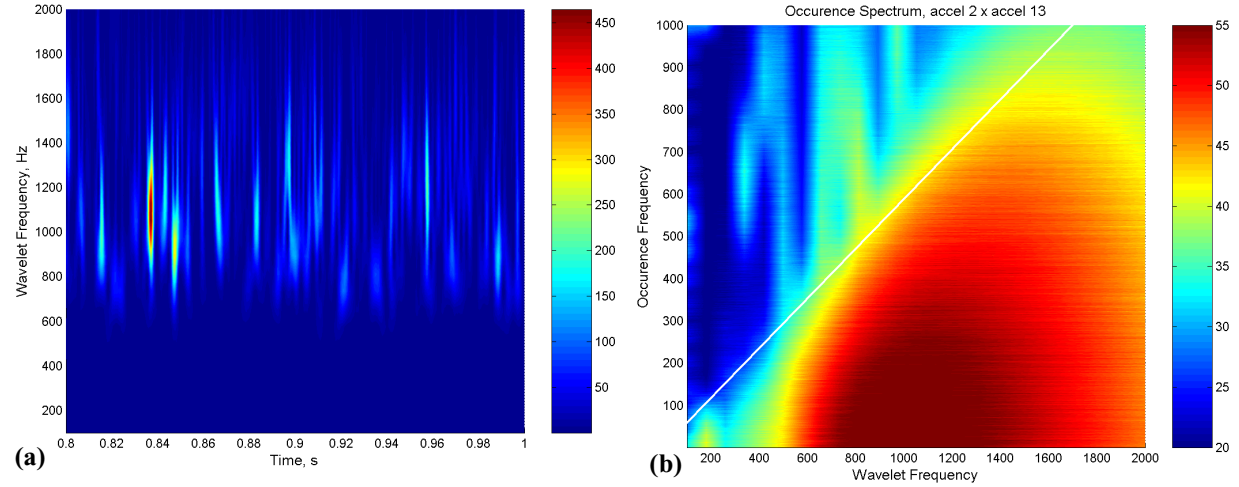

Figure 15. CWT of upstream accelerometer (accel 2), (a), and, occurrence spectrum of XWT between accel 2 and accel 13, with white line denoting an occurrence limit of 0.6 the wavelet frequency, (b).

VIII. Conclusions

The techniques introduced in this study have been shown to be useful in detecting and evaluating the existence of persistent structures in the turbulent boundary layer. Persistent structures have been shown to be 10 to 20 cm. in size and to exist for up to 50 cm. The structures exist with frequency content in the range from 250 to 2000 Hz and can account for up to 95% of the coherent power in the TBL at separations of 20 cm. Structures that occur at lower rates are shown to contain greater power. These results establish a basis for a numerical study of the interaction of pressure profiles, such as those described here, with sidewall structures typical of airframe construction to determine if these structures could indeed be a major source of vibration energy in the aircraft sidewall.

IX. Acknowledgement

The author would like to thank Lucio Maestrello for his insight into these phenomena, his inspiration to use unconventional analysis and his example of tireless enthusiasm in pursuit of one's vision.

X. References

[1]Graham, W.R., "A Comparison of Models for the Wavenumber-Frequency Spectrum of Turbulent Boundary Layer Pressures", *Journal of Sound and Vibration*, Vol 206(4), 1997, pp. 541-565.

[2]Maury, C.,Gardonio, P. and Elliott, S.J., "A Wavenumber Approach to Modelling the Response of a Randomly Excited Panel, Part I", *Journal of Sound and Vibration*, Vol. 252(1), 2002, pp. 83-113.

[3]Addison, P.S., Watson, J.N., and Feng, T., "Low Oscillation Complex Wavelets", *Journal of Sound and Vibration*, Vol. 254(4), 2002, pp. 733-762.

[4]Daubechies, I., "Ten lectures on wavelets", 1992, SIAM.

[5]Wusk, M.S., "ARIES: NASA Langley's Airborne Research Facility", *AIAA's Aircraft Technology, Integration, and Operations (ATIO) 2002 Technical Forum,* AIAA 2002-5822, Los Angeles, CA, 2002, pp. 11.